PROCEEDINGS OF SCIENCE

Saturation physics with prompt photons at NLO in $p+A$ collisions

Sanjin Benić*
Yukawa Institute for Theoretical Physics, Kyoto University, Kyoto 606-8502, Japan
Physics Department, Faculty of Science, University of Zagreb, Zagreb 10000, Croatia
E-mail: benic.sanjin@yukawa.kyoto-u.ac.jp

Oscar Garcia-Montero
Institut für Theoretische Physik, Universität Heidelberg, Philosophenweg 16, 69120 Heidelberg, Germany
E-mail: garcia@thphys.uni-heidelberg.de

We present recent progress in the analytical as well as the numerical calculation of the next-to-leading order (NLO) inclusive photon production and photon-jet angular correlations at central rapidities applicable to $p+A$ and $p+p$ collisions. After explaining the general cross section formulae we analyze numerically the different NLO contributions. We quantify the importance of quantum evolution effects for the gluon distribution functions. Finally, we show the results on photon-jet angular harmonics as a probe of gluon saturation effects.

12th International Workshop on High-pT Physics in the RHIC/LHC Era
2-5 October, 2017
University of Bergen, Bergen, Norway

*Speaker.

https://pos.sissa.it/

PoS(High-pT2017)021

1. Introduction

Gluons are the dominant component of the hadron wavefunction at high energy (or small-x). Large gluon occupation numbers are treated within a semi-classical framework, called the Color Glass Condensate (CGC) [1, 2, 3] where all-order rescatterings with a dense target and non-linear quantum evolutions are taken into account. In particular, this leads to a generalization of the gluon distribution functions through which gluons acquire finite transverse momenta with typical values $k_\perp \sim Q_S(x)$, where $Q_S(x)$ is the saturation scale at some momentum fraction x.

Photons are sensitive to high density gluon effects through their couplings to quarks. As opposed to hadron production, inclusive photon production does not suffer from uncertainties related to hadronization mechanisms. Even for semi-inclusive reactions $h_1 + h_2 \to a + b + X$, where at least a or b is the photon, such uncertainties become reduced.

The leading order (LO) photon production in the CGC framework for the $p+A$ collisions is obtained from the channel $q \to q\gamma$ [4, 5, 6] (in the A background), that would be important at forward photon rapidities, η_{k_γ} and/or large photon transverse momenta, where the projectile proton momentum fraction, $x_p \sim \frac{k_{\gamma\perp}}{\sqrt{s}} e^{\eta_{k_\gamma}}$, can be large. With current collider energies in the TeV range, x_p can be of the order of $x_p \sim 10^{-3} - 10^{-4}$ so that the gluons in the projectile become dominant, leading to new inclusive photon production channels. Although formally next-to-leading order (NLO) in α_S they would dominate over the LO contribution at central rapidities and/or high energy.

2. NLO photon cross section

The NLO contributions come from the exclusive $g \to q^* \bar{q}^* \to \gamma$ channel, the $g \to q\bar{q}\gamma$ and the $q \to qg\gamma$ channel. Below we give main analytical results for the $g \to \gamma$ and the $g \to q\bar{q}\gamma$ channel, as obtained in [7] and [8], respectively. For $q \to qg\gamma$, the collinearly enhanced parts are absorbed at LO through parton evolution, while the magnitude of the non-collinearly enhanced parts depend in general on the renormalization and the factorization scale and on the quark distribution $f_q(x,Q^2)$, as opposed to the gluon distribution $f_g(x,Q^2)$, of the projectile. In this work, we consider the kinematic region where $f_q(x,Q^2) \ll f_g(x,Q^2)$, while $f_g(x,Q^2) < 1/\alpha_S$.

The $g \to \gamma$ channel proceeds through a loop with virtual quarks $q^*\bar{q}^*$, that annihilate to a photon in the final state. The cross section is [7]

$$\begin{aligned}
\frac{d\sigma^{g\to\gamma}}{d^2\boldsymbol{k}_{\gamma\perp} d\eta_{k_\gamma}} = {} & \frac{\alpha_e \alpha_S}{64\pi^8 C_F} \int_{xx'} \int_{\boldsymbol{y}_\perp \boldsymbol{y}'_\perp \boldsymbol{z}_\perp \boldsymbol{z}'_\perp} \int_{\boldsymbol{k}_{1\perp}} e^{-i(\boldsymbol{k}_{1\perp} - \boldsymbol{k}_{\gamma\perp})\cdot(\bar{x}\boldsymbol{y}_\perp + x\boldsymbol{z}_\perp - \bar{x}'\boldsymbol{y}'_\perp - x'\boldsymbol{z}'_\perp)} \varphi_p(Y_p, \boldsymbol{k}_{1\perp}) \\
& \times \left[\mathcal{Q}_{A,Y_A}(\boldsymbol{y}_\perp, \boldsymbol{y}'_\perp, \boldsymbol{z}'_\perp, \boldsymbol{z}_\perp) - \tilde{\mathcal{N}}_{A,Y_A}(\boldsymbol{y}_\perp - \boldsymbol{z}_\perp)\tilde{\mathcal{N}}_{A,Y_A}(\boldsymbol{y}'_\perp - \boldsymbol{z}'_\perp)\right] \\
& \times \sum_{f,f'} q_f q_{f'} \left[\hat{\boldsymbol{u}}_\perp \Psi_{1,f}(\boldsymbol{k}_{1\perp}, \boldsymbol{u}_\perp, x) + \hat{\boldsymbol{k}}_{1\perp} \Psi_{2,f}(\boldsymbol{k}_{1\perp}, \boldsymbol{u}_\perp, x)\right] \\
& \times \left[\hat{\boldsymbol{u}}_\perp \Psi^*_{1,f'}(\boldsymbol{k}_{1\perp}, \boldsymbol{u}'_\perp, x') + \hat{\boldsymbol{k}}_{1\perp} \Psi^*_{2,f'}(\boldsymbol{k}'_{1\perp}, \boldsymbol{u}'_\perp, x')\right] ,
\end{aligned} \tag{2.1}$$

PoS(High-pT2017)021

where $\int_x \equiv \int_0^1 dx$, $\bar{x} \equiv 1-x$ and $\boldsymbol{u}_\perp \equiv \boldsymbol{z}_\perp - \boldsymbol{y}_\perp$ and similar for the primed coordinates, while $\hat{\boldsymbol{x}}_\perp \equiv \boldsymbol{x}_\perp/x_\perp$. Here the gluons in the nuclei in the $g \to \gamma$ process are described through the dipole $\tilde{\mathcal{N}}_{A,Y_A}(\boldsymbol{y}_\perp - \boldsymbol{z}_\perp)$ and the quadrupole distribution $\mathcal{Q}_{A,Y_A}(\boldsymbol{y}_\perp, \boldsymbol{y}'_\perp, \boldsymbol{z}'_\perp, \boldsymbol{z}'_\perp)$, while the gluons in the proton are described by the familiar un-integrated gluon distribution $\varphi_p(Y_p, \boldsymbol{k}_{1\perp})$. The explicit forms of the functions $\Psi_{(1,2),f}(\boldsymbol{k}_{1\perp}, \boldsymbol{u}_\perp, x)$ are given in [7].

The fully differential cross section for the $g \to q\bar{q}\gamma$ channel was calculated in [8], where the most general form was found as

$$
\begin{aligned}
\frac{\mathrm{d}\sigma^{g\to q\bar{q}\gamma}}{\mathrm{d}^2\boldsymbol{k}_{\gamma\perp}\mathrm{d}\eta_{k_\gamma}\mathrm{d}^2\boldsymbol{q}_\perp \mathrm{d}\eta_q \mathrm{d}^2\boldsymbol{p}_\perp \mathrm{d}\eta_p} &= \frac{\alpha_e \alpha_S^2}{256\pi^8 C_F}\sum_f q_f^2 \int_{\boldsymbol{k}_{1\perp}\boldsymbol{k}_{2\perp}} (2\pi)^2 \delta^{(2)}(\boldsymbol{P}_\perp - \boldsymbol{k}_{1\perp} - \boldsymbol{k}_{2\perp}) \\
&\times \frac{\varphi_p(Y_p, \boldsymbol{k}_{1\perp})}{\boldsymbol{k}_{1\perp}^2 \boldsymbol{k}_{2\perp}^2} \Big\{ \tau_{g,g}(\boldsymbol{k}_{1\perp}; \boldsymbol{k}_{1\perp}) \phi_A^{g,g}(Y_A, \boldsymbol{k}_{2\perp}) \\
&+ 2\int_{\boldsymbol{k}_\perp} \tau_{g,q\bar{q}}(\boldsymbol{k}_{1\perp}; \boldsymbol{k}_\perp, \boldsymbol{k}_{1\perp})\, \phi_A^{q\bar{q},g}(Y_A, \boldsymbol{k}_\perp, \boldsymbol{k}_{2\perp} - \boldsymbol{k}_\perp; \boldsymbol{k}_{2\perp}) \\
&+ \int_{\boldsymbol{k}_\perp \boldsymbol{k}'_\perp} \tau_{q\bar{q},q\bar{q}}(\boldsymbol{k}_\perp, \boldsymbol{k}_{1\perp}; \boldsymbol{k}'_\perp, \boldsymbol{k}_{1\perp})\, \phi_A^{q\bar{q},q\bar{q}}(Y_A, \boldsymbol{k}_\perp, \boldsymbol{k}_{2\perp} - \boldsymbol{k}_\perp; \boldsymbol{k}'_\perp, \boldsymbol{k}_{2\perp} - \boldsymbol{k}'_\perp) \Big\},
\end{aligned}
\tag{2.2}
$$

where $\phi_A^{m,n}$ are the multi-gluon correlators describing the distribution in the saturated target, while $\tau_{n,m}$ are the appropriate hard factors (explicit expressions can be found in [8]). The multi-gluon correlators were first introduced in [9] for $q\bar{q}$ production in $p+A$ collisions. There it was demonstrated that $\phi_A^{q\bar{q},q\bar{q}}$ involves a product of four Wilson lines in the fundamental representation, while $\phi_A^{q\bar{q},g}$ a product of two Wilson lines in the fundamental and a Wilson line in the adjoint representation, while $\phi_A^{g,g}$ involves a product of two Wilson lines in the adjoint representation. At large N_c these distributions simplify to a product of dipoles $\tilde{\mathcal{N}}_{A,Y_A}(\boldsymbol{k}_\perp)$ defined as

$$
\tilde{\mathcal{N}}_{A,Y_A}(\boldsymbol{k}_\perp) = \frac{1}{N_c}\int_{\boldsymbol{x}_\perp} \mathrm{e}^{i\boldsymbol{k}_\perp \cdot \boldsymbol{x}_\perp} \mathrm{tr}_c \langle \tilde{U}(\boldsymbol{x}_\perp)\tilde{U}^\dagger(0)\rangle_{Y_A}\,, \tag{2.3}
$$

where $\tilde{U}(\boldsymbol{x}_\perp)$ is the fundamental Wilson line, and $\langle\cdots\rangle_{Y_A}$ denotes a quantum average to be calculated with the appropriate weight functional and satisfying the general JIMWLK evolution equations. The inclusive cross section from Eq. (2.2) becomes

$$
\begin{aligned}
\frac{1}{\pi R_p^2 \pi R_A^2}\frac{\mathrm{d}\sigma^{g\to q\bar{q}\gamma}}{d^2\boldsymbol{k}_{\gamma\perp} d\eta_{k_\gamma}} &= \frac{\alpha_e N_c^3}{128\pi^4 (N_c^2-1)}\sum_f q_f^2 \int_{\eta_q \eta_p}\int_{\boldsymbol{q}_\perp \boldsymbol{p}_\perp \boldsymbol{k}_{1\perp}\boldsymbol{k}_\perp} \mathcal{N}_{p,Y_p}(\boldsymbol{k}_{1\perp}) \\
&\times \tilde{\mathcal{N}}_{A,Y_A}(\boldsymbol{k}_\perp)\tilde{\mathcal{N}}_{A,Y_A}(\boldsymbol{P}_\perp - \boldsymbol{k}_{1\perp} - \boldsymbol{k}_\perp) \\
&\times [\tau_{g,g}(\boldsymbol{k}_{1\perp}; \boldsymbol{k}_{1\perp}) + 2\tau_{g,q\bar{q}}(\boldsymbol{k}_{1\perp}; \boldsymbol{k}_\perp, \boldsymbol{k}_{1\perp}) + \tau_{q\bar{q},q\bar{q}}(\boldsymbol{k}_\perp, \boldsymbol{k}_{1\perp}; \boldsymbol{k}_\perp, \boldsymbol{k}_{1\perp})]\,,
\end{aligned}
\tag{2.4}
$$

where we used $\varphi_p(Y_p, \boldsymbol{k}_{1\perp}) \equiv (\pi R_p^2)\frac{N_c \boldsymbol{k}_{1\perp}^2}{4\alpha_S}\mathcal{N}_{p,Y_p}(\boldsymbol{k}_{1\perp})$ for the gluon distribution in the projectile proton, with $\mathcal{N}_{p,Y_p}(\boldsymbol{k}_{1\perp})$ as the adjoint dipole.

3. NLO Inclusive photon production - selected numerical results

Here we show several preliminary numerical results of the calculation of the inclusive photon cross section in $p+p$ collisions. It is useful to compare the magnitude of the NLO

PoS(High-pT2017)021

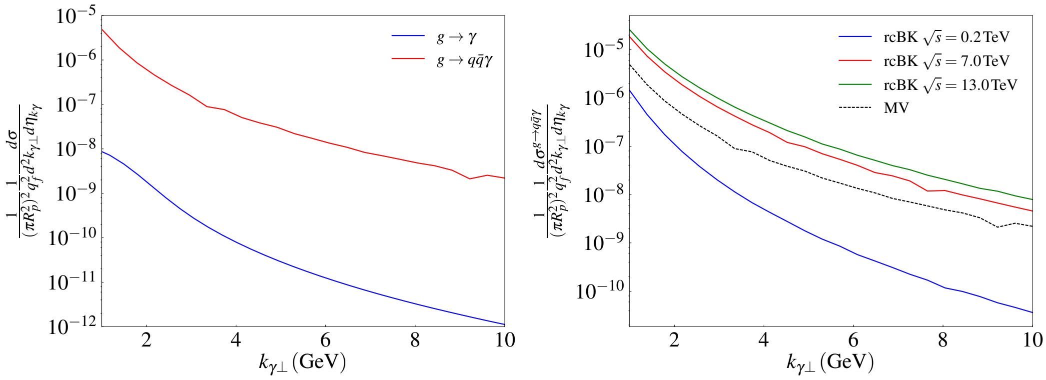

Figure 1: Left panel: comparison of the NLO $g \to \gamma$ and $g \to q\bar{q}\gamma$ transverse photon momentum ($k_{\gamma\perp}$) dependence of the inclusive photon cross section in $p+p$ collisions using the MV model (3.1) for the gluon distributions. Right panel: comparison of inclusive $g \to q\bar{q}\gamma$ cross section in $p+p$ at central rapidity and for several collision energies $\sqrt{s}$ using the rcBK solutions for the gluon distributions. The results are shown for a single flavor with mass $m_f = 0.2$ GeV.

channels $g \to \gamma$ and $g \to q\bar{q}\gamma$. For the moment we simplify our approach by using a classical McLerran-Venugopalan (MV) model [10, 11] to calculate the gluon distributions, so that

$$\mathcal{N}(\boldsymbol{x}_\perp) = \exp\left[-\frac{(x_\perp^2 Q_{S0}^2)^\gamma}{2} \log\left(\frac{1}{x_\perp \Lambda_{\rm IR}} + {\rm e}\right)\right]. \tag{3.1}$$

We use the parameters $\gamma = 1$, $Q_{S0}^2 = 0.2$ GeV^2, $\Lambda_{\rm IR} = 0.241$ GeV. A separable form of the quadrupole $\mathcal{Q}(\boldsymbol{y}_\perp, \boldsymbol{y}'_\perp, \boldsymbol{z}'_\perp, \boldsymbol{z}'_\perp)$ was found [12] to be a good approximation and we use it in this work. We used a single quark flavor with mass $m_f = 0.2$ GeV. The result on the left panel of Fig. 1 demonstrates in a clear way that, due to the restricted phase space of the virtual $q^*\bar{q}^*$, the $g \to \gamma$ channel is greatly suppressed relative to $g \to q\bar{q}\gamma$. Taking into account all quark flavors there are even more suppressions due to the strong cancellations of the different flavor contributions, see Eq. (2.1).

We implement the quantum evolution of the distributions using the solutions of the running coupling Balitsky-Kovchegov (rcBK) equation [13, 14, 15, 16] with the initial condition (3.1) at $x = 10^{-2}$, as obtained in [17]. The results are shown on the right panel of Fig. 1, where we again use a single flavor with $m_f = 0.2$ GeV at collision energies $\sqrt{s} = 0.2$, 7 and 13 TeV and central rapidity $\eta_{k_\gamma} = 0.0$.

The result at 0.2 TeV is different from the result using only the MV model, without the initial condition. As the relevant kinematic region is mostly $x > 10^{-2}$ this is not the quantum evolution effect, but rather the large-x physics effect, with the rcBK solutions extrapolated to large-x region $x > 10^{-2}$ as in [12], not present in the MV model. We can see the rcBK evolution effect at 7 and 13 TeV where the cross section now considerably deviates from the calculation using the initial condition.

4. Photon-jet angular correlations

The calculation of the photon-jet angular correlations was carried out in [18]. Using the transverse momenta variables

$$\boldsymbol{Q}_\perp = \boldsymbol{p}_\perp + \boldsymbol{k}_{\gamma\perp} \qquad \tilde{\boldsymbol{P}}_\perp = \frac{\boldsymbol{p}_\perp - \boldsymbol{k}_{\gamma\perp}}{2}\,, \tag{4.1}$$

we consider almost back-to-back events as $Q_\perp \ll \tilde{P}_\perp$, where $Q_\perp$ should be understood as a soft scale scale (in this context $Q_\perp \sim Q_S$) while $\tilde{P}_\perp$ is a hard scale.

The LO cross section, when expressed in the back-to-back variables, is isotropic to $Q_\perp^2/Q_S^2$, with angular dependence arising only at $(Q_\perp^2/Q_S^2)\times(Q_\perp/\tilde{P}_\perp)$ [18]. Intuitively, at LO the back-to-back (or *anti*-collinear) correlations are suppressed in the CGC regime, as the photon would dominantly be emitted collinear to its parent quark. Thanks to the three body final state at NLO we can consider collinear photon emission from the parent quark and check for back-to-back correlations with the remaining antiquark (or vice versa).

Due to the presence of a hard scale, we are able to simplify further the general NLO expression for the cross section (2.2). The gluon distributions of the target appear in the form of various transverse momentum distributions [19, 20] $F_i(x_A,\boldsymbol{k}_\perp^2)$ and $H_i(x_A,\boldsymbol{k}_\perp^2)$ where $i=1,\ldots,3$ and $F_i(H_i)$ are the distributions of unpolarized (linearly polarized) gluons. Integrating over the parent quark momenta $\boldsymbol{q}_\perp$, our final expression takes the form

$$\begin{aligned}
\frac{d\sigma}{d^2\tilde{\boldsymbol{P}}_\perp d^2\boldsymbol{Q}_\perp d\eta_p d\eta_{k_\gamma} dz} &= \frac{\alpha_e \alpha_S q_f^2}{64\pi^4 N_c(N_c^2-1)} x_p f_{g,p}\left(x_p,\boldsymbol{P}_\perp^2\right)\frac{1}{2\pi}\frac{1+(1-z)^2}{z}\log\left(\frac{\boldsymbol{P}_\perp^2}{\Lambda^2_{\overline{\rm MS}}}\right)\\
&\times \frac{\zeta(1+z)^4}{z(\zeta+z)^6}\frac{1}{\tilde{P}_\perp^4}\Bigg\{(\zeta^4+6\zeta^2z^2+z^4)F_1\left(x_A,\boldsymbol{P}_\perp^2\right) - 2\zeta z(\zeta-z)^2 F_2\left(x_A,\boldsymbol{P}_\perp^2\right) - 4\zeta^2z^2F_3\left(x_A,\boldsymbol{P}_\perp^2\right)\\
&+4\zeta z(\zeta-z)^2\left[\frac{(\boldsymbol{P}_\perp\cdot\tilde{\boldsymbol{P}}_\perp)^2}{\boldsymbol{P}_\perp^2\tilde{\boldsymbol{P}}_\perp^2}-\frac{1}{2}\right]\left[-H_1\left(x_A,\tilde{\boldsymbol{P}}_\perp^2\right)-H_2\left(x_A,\boldsymbol{P}_\perp^2\right)+H_3\left(x_A,\boldsymbol{P}_\perp^2\right)\right]\Bigg\}.
\end{aligned} \tag{4.2}$$

where $z = k_\gamma^+/(k_\gamma^+ + q^+)$, $\zeta = p^+/k_\gamma^+$ and $\boldsymbol{P}_\perp = (-(1-z)\tilde{\boldsymbol{P}}_\perp + (1+z)\boldsymbol{Q}_\perp/2)/z$. We are considering events where z is close to unity so that photon takes most of the momentum from the parent quark. It turns out that the particular combination of H_i in Eq. (4.2) vanishes [18].

Expanding (4.2) in powers of $Q_\perp/\tilde{P}_\perp$ we can extract the angular correlations as $a_n = \langle\cos(n\phi)\rangle$ where ϕ is the angle between $\boldsymbol{Q}_\perp$ and $\tilde{\boldsymbol{P}}_\perp$. By contrast to LO, the anisotropic contribution to the cross section starts at $Q_\perp/\tilde{P}_\perp$. The angular harmonics have an overall $a_n \sim (Q_\perp/\tilde{P}_\perp)^n$ dependence. For example, the explicit expression for a_1 is [18]

$$a_1 = \frac{1+z}{4(1-z)}\frac{Q_\perp}{\tilde{P}_\perp}\frac{(\zeta^4+6\zeta^2z^2+z^4)F_1^{(1,1)} - 2\zeta z(\zeta-z)^2F_2^{(1,1)} - 4\zeta^2z^2F_3^{(1,1)}}{(\zeta^4+6\zeta^2z^2+z^4)F_1 - 2\zeta z(\zeta-z)^2F_2 - 4\zeta^2z^2F_3} + O\left(Q_\perp^3/\tilde{P}_\perp^3\right), \tag{4.3}$$

with $F_i^{(a,b)} = F_i^{(a,b)}(x_A,(1-z)^2\tilde{P}_\perp^2/z^2)$ are the moments of the distributions F_i. Even though $\tilde{P}_\perp$ is hard, since $1-z \ll 1$, the argument of the distribution functions is sensitive to scales appropriate for exploring saturation effects. On Fig. 2 we show results for a_1 using the MV model. Results for a_2 are qualitatively similar, but overall suppressed due to the $Q_\perp^2/\tilde{P}_\perp^2$ prefactor.

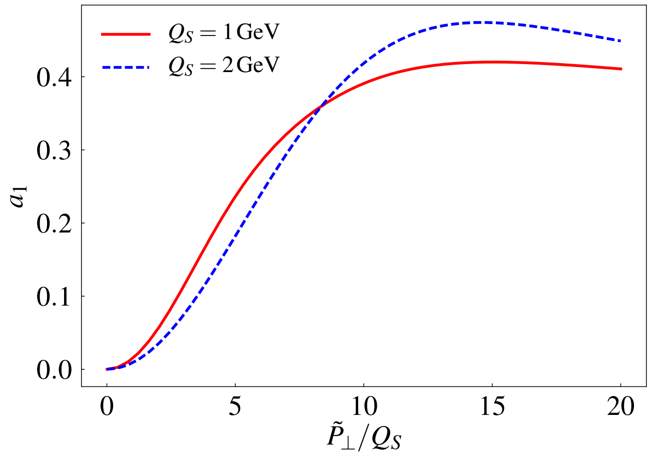

Figure 2: Angular correlation a_1 for inclusive $g \to q\gamma$ to order $Q_\perp^2/\tilde{P}_\perp^2$ using the MV model with two different saturation scales. We take $Q_\perp/\tilde{P}_\perp = 0.1$, $z = 3/4$ and $\zeta = 1$. Fig. from [18].

5. Conclusions

We have calculated complete analytical result for the photon production at NLO in the CGC framework. We have found that $g \to \gamma$ is numerically much smaller than the $g \to q\bar{q}\gamma$ channel due to phase space restrictions. For LHC phenomenology it is important to take into account the effects of quantum evolution. In the case of photon-jet final state we have found interesting all-orders azimuthal harmonics from back-to-back kinematics sensitive to the saturation physics.

Acknowledgments

We would like to thank our colleagues Kenji Fukushima and Raju Venugopalan for collaborations. We thank Kevin Dusling for his help with the rcBK solutions. S. B. thanks Adrian Dumitru for collaboration. S. B. acknowledges discussions with Yoshitaka Hatta and Davor Horvatić. S. B. was supported by the European Union Seventh Framework Programme (FP7 2007-2013) under grant agreement No. 291823, Marie Curie FP7-PEOPLE2011-COFUND NEWFELPRO Grant No. 48. S. B. is supported by the JSPS fellowship and JSPS Grant-in-Aid for JSPS fellows 17F17323. S. B. acknowledges HRZZ Grant No. 8799 at the University of Zagreb for computational resources. This work is part of and supported by the DFG Collaborative Research Centre "SFB 1225 (ISOQUANT)".

References

[1] E. Iancu and R. Venugopalan, *The Color glass condensate and high-energy scattering in QCD*, in *In *Hwa, R.C. (ed.) et al.: Quark gluon plasma* 249-3363*. 2003. hep-ph/0303204. DOI.

[2] J. Jalilian-Marian and Y. V. Kovchegov, *Saturation physics and deuteron-Gold collisions at RHIC*, *Prog. Part. Nucl. Phys.* **56** (2006) 104–231, [hep-ph/0505052].

[3] F. Gelis, E. Iancu, J. Jalilian-Marian and R. Venugopalan, *The Color Glass Condensate*, *Ann. Rev. Nucl. Part. Sci.* **60** (2010) 463–489, [1002.0333].

[4] B. Z. Kopeliovich, A. V. Tarasov and A. Schafer, *Bremsstrahlung of a quark propagating through a nucleus*, *Phys. Rev.* **C59** (1999) 1609–1619, [hep-ph/9808378].

[5] F. Gelis and J. Jalilian-Marian, *Photon production in high-energy proton nucleus collisions*, *Phys. Rev.* **D66** (2002) 014021, [hep-ph/0205037].

[6] R. Baier, A. H. Mueller and D. Schiff, *Saturation and shadowing in high-energy proton nucleus dilepton production*, *Nucl. Phys.* **A741** (2004) 358–380, [hep-ph/0403201].

[7] S. Benic and K. Fukushima, *Photon from the annihilation process with CGC in the pA collision*, *Nucl. Phys.* **A958** (2017) 1–24, [1602.01989].

[8] S. Benic, K. Fukushima, O. Garcia-Montero and R. Venugopalan, *Probing gluon saturation with next-to-leading order photon production at central rapidities in proton-nucleus collisions*, *JHEP* **01** (2017) 115, [1609.09424].

[9] J. P. Blaizot, F. Gelis and R. Venugopalan, *High-energy pA collisions in the color glass condensate approach. 2. Quark production*, *Nucl. Phys.* **A743** (2004) 57–91, [hep-ph/0402257].

[10] L. D. McLerran and R. Venugopalan, *Computing quark and gluon distribution functions for very large nuclei*, *Phys. Rev.* **D49** (1994) 2233–2241, [hep-ph/9309289].

[11] L. D. McLerran and R. Venugopalan, *Gluon distribution functions for very large nuclei at small transverse momentum*, *Phys. Rev.* **D49** (1994) 3352–3355, [hep-ph/9311205].

[12] Y.-Q. Ma and R. Venugopalan, *Comprehensive Description of J/ÏĹ Production in Proton-Proton Collisions at Collider Energies*, *Phys. Rev. Lett.* **113** (2014) 192301, [1408.4075].

[13] I. Balitsky, *Operator expansion for high-energy scattering*, *Nucl. Phys.* **B463** (1996) 99–160, [hep-ph/9509348].

[14] Y. V. Kovchegov, *Small x F(2) structure function of a nucleus including multiple pomeron exchanges*, *Phys. Rev.* **D60** (1999) 034008, [hep-ph/9901281].

[15] J. L. Albacete, N. Armesto, J. G. Milhano and C. A. Salgado, *Non-linear QCD meets data: A Global analysis of lepton-proton scattering with running coupling BK evolution*, *Phys. Rev.* **D80** (2009) 034031, [0902.1112].

[16] J. L. Albacete, N. Armesto, J. G. Milhano, P. Quiroga-Arias and C. A. Salgado, *AAMQS: A non-linear QCD analysis of new HERA data at small-x including heavy quarks*, *Eur. Phys. J.* **C71** (2011) 1705, [1012.4408].

[17] K. Dusling, F. Gelis, T. Lappi and R. Venugopalan, *Long range two-particle rapidity correlations in A+A collisions from high energy QCD evolution*, *Nucl. Phys.* **A836** (2010) 159–182, [0911.2720].

[18] S. Benic and A. Dumitru, *Prompt photon - jet angular correlations at central rapidities in p+A collisions*, *Phys. Rev.* **D97** (2018) 014012, [1710.01991].

[19] C. J. Bomhof, P. J. Mulders and F. Pijlman, *The Construction of gauge-links in arbitrary hard processes*, *Eur. Phys. J.* **C47** (2006) 147–162, [hep-ph/0601171].

[20] E. Akcakaya, A. SchÃďfer and J. Zhou, *Azimuthal asymmetries for quark pair production in pA collisions*, *Phys. Rev.* **D87** (2013) 054010, [1208.4965].